Robust Estimation of the Discrete Spectrum of Relaxations for Electromagnetic Induction Responses

Mu-Hsin Wei, *Student Member, IEEE*, Waymond R. Scott, Jr., *Fellow, IEEE*, and James H. McClellan, *Fellow, IEEE*

***Abstract*—The electromagnetic induction response of a target can be accurately modeled by a sum of real exponentials. However, it is difficult to obtain the model parameters from measurements when the number of exponentials in the sum is unknown or the terms are strongly correlated. Traditionally, the time constants and residues are estimated by nonlinear iterative search. In this paper, a constrained linear method of estimating the parameters is formulated by enumerating the relaxation parameter space and imposing a nonnegative constraint on the parameters. The resulting algorithm does not depend on a good initial guess to converge to a solution. By using tests on synthetic data and laboratory measurement of known targets, the proposed method is shown to provide accurate and stable estimates of the model parameters.**

***Index Terms*—Discrete spectrum of relaxation frequencies (DSRFs), electromagnetic induction (EMI), magnetic polarizabilities, sum of exponentials.**

I. Introduction

ELECTROMAGNETIC induction (EMI) sensors work by illuminating a target of interest with a time-varying magnetic field and then detecting the scattered magnetic field which is generated by the eddy currents induced on the target. Recent research has shown that advanced EMI sensors, which measure the scattered field at a broad range of frequencies or measurement times, are capable of discriminating between certain types of targets [1]–[3]. Target discrimination is realizable because the measurements are strongly related to the target's physical size, shape, orientation, and composition. In a broadband system, it is possible that measurements at a small number of frequencies are sufficient to represent a target. Several researchers have demonstrated subsurface target discrimination based on the EMI response [4], [5].

Several different approaches have been developed to analyze the EMI response of targets. Miller *et al.* [6] proposed a three-parameter model for targets of compact shapes and a four-parameter model as its extension. The measured frequency response can be approximated by fitting the parameters of these models, and then, identification is performed based on the fitted parameters. Many others have worked out the theoretical model for the response of canonical targets [7], [8]. These models, however, do not appropriately describe objects with more general shapes.

Interestingly, the dielectric response of materials has similar characteristics to the EMI frequency response. Thus, models and methods developed for dielectric materials can be applied to the EMI response. One advantage of doing so is that many of the dielectric models and methods have been well studied over the past 50 years and that much is known about the behavior and properties of the models. For example, the parametric model proposed by Miller *et al.* can be rewritten in the form of the Cole–Cole dielectric relaxation model [9]. Other parametric models well known in polymer science, such as the Havriliak–Negami and Cole–Davidson models, could also be used in modeling the EMI response of targets with more complex shapes [10], [11].

A. DRT

One analysis tool used in polymer science to characterize materials is expressing the dielectric response in terms of a distribution of relaxation times (DRT) [12]. The DRT can reveal characteristics of materials that are not obvious in the raw measurements. Because the DRT representation makes less assumptions about the structure of the response, it offers a model that is more general than the parametric models. The normalized DRT $G(\tau)$ is defined as

$$H(\omega) = g_0 + g_\Delta \int_0^\infty \frac{G(\tau)}{1 + j\omega\tau}\, d\tau \tag{1}$$

where $H(\omega)$ is the frequency response, τ is the relaxation time, and g_0 and g_Δ are constants. The DRT $G(\tau)$ is normalized to have unity area.

The DRT of some parametric models can be derived analytically. For example, the Cole–Cole model (hence, Miller's model) [13] is

$$H_{\mathrm{CC}}(\omega) = g_0 + \frac{g_\Delta}{1 + (j\omega\tau_0)^\alpha} \tag{2}$$

$$G_{\mathrm{CC}}(\tau) = \frac{1}{2\pi\tau} \frac{\sin(\alpha\pi)}{\cosh\left(\alpha \log(\tau/\tau_0)\right) + \cos(\alpha\pi)} \tag{3}$$

where τ_0 and α are model parameters. Here, $G_{\mathrm{CC}}(\tau)$ is restricted to be symmetric with respect to τ_0 in log-τ space because of the assumed structure of H_{CC}. In describing a target response with a parametric model, details and features may be lost in the fitting process. For example, not all targets have symmetric DRTs. Using Cole–Cole to model such targets would result in a loss of information. Describing a target directly in terms of its DRT can be more accurate.

Manuscript received December 2, 2008; revised May 29, 2009. First published October 6, 2009; current version published February 24, 2010. This work was supported in part by the U.S. Army Night Vision and Electronic Sensors Directorate, Science and Technology Division, Countermine Branch, and in part by the U.S. Army Research Office under Contract W911NF-05-1-0257.

The authors are with the School of Electrical and Computer Engineering, Georgia Institute of Technology, Atlanta, GA 30332-0250 USA (e-mail: gth879w@mail.gatech.edu; waymond.scott@ece.gatech.edu; jim.mcclellan@ece.gatech.edu).

Digital Object Identifier 10.1109/TGRS.2009.2029981

B. DSRF

In the study of EMI, several researchers have provided a theoretical basis for representing the EMI response of a metallic object as a discrete sum of damped real exponentials [14], [15]. In terms of the DRT, an EMI response can be represented by (1) with a *discrete* DRT. In addition, we have found that it is more intuitive and convenient to write (1) in terms of *relaxation frequencies* rather than relaxation times. By using the notation of relaxation frequency, we can rewrite (1) in discrete form as

$$H(\omega) = c_0 + \sum_{k=1}^{K} \frac{c_k}{1 + j\omega/\zeta_k} \tag{4}$$

where c_0 is the shift, K is the model order, c_k is the real spectral amplitudes, and $\zeta_k = 1/\tau_k$ are the relaxation frequencies. The shape of the EMI frequency response of a target can be precisely represented by the set $S = \{(\zeta_k, c_k) : k = 1, \ldots, K\}$ which we will call the discrete spectrum of relaxation frequencies (DSRFs). Each pair (ζ_k, c_k) is one relaxation. The parameter c_0 is not considered to be part of the DSRF because it is just a shift of the frequency response. The response at zero frequency $H(0) = \sum_{k=0}^{K} c_k$ is due to the dc magnetization of the target. The term DSRF and spectrum will be used interchangeably throughout this paper.

The frequency response $H(\omega)$ is proportional to the projection of the magnetic polarizability tensor of the target being measured by the EMI sensor. The magnetic polarizability, hence the DSRF, of several canonical targets can be calculated analytically, and these formulas show how the DSRF is related to the target's physical properties such as conductivity, permeability, shape, size, and orientation [16]–[18].

The DSRF representation has several useful properties. Not only is the DSRF an alternative to representing a target response but also it is directly related to the physical properties of a target. In addition, the relaxation frequencies of a target are invariant to its relative orientation and position to the sensor. Only the spectral amplitudes change with orientation and position, and this makes the DSRF a valuable feature for target discrimination. Baum has coined the term "magnetic singularity identification" when using the relaxations (singularities) for identifying targets.

C. Difficulties

While modeling the EMI response in terms of a distribution is of great value in examining target characteristics, estimating the DRT, both continuous and discrete, from the frequency response is not straightforward. Many methods have been developed in many fields of science for solving such problems. In the case of a continuous DRT, one solves a Fredholm integral equation of the first kind. Methods such as Tikhonov regularization [19], a nonparametric Bayesian approach [20], and a Monte Carlo method [21] could be useful. In the discrete case, the problem is to find the parameters of a sum of exponentials. Techniques such as iterative nonlinear least squares (LSQ) fitting, the matrix pencil method, and modified Prony's methods have been used in the past [22], [23]. Often, these methods do not perform well when three or more relaxations are present. The goodness of fit strongly depends on a good guess of the model order and is also very sensitive to the initial guess for the model parameters. More discussion on the performance of these methods can be found in [5] and [24].

In practice, a good initial guess is hard to determine, and it is difficult, if not impossible, to have prior knowledge on the model order. For these reasons, most existing estimation methods are prone to not converging in the fitting process. Even if the fitting method converges well with a small residual, there is the concern that the estimated relaxations could be very different from the actual ones. It is possible that the estimate is merely a good numerical fit, but has no physical significance [24].

One robust spectrum estimation method is the MATLAB function `invfreqs` which implements the algorithm proposed by Levy [25]. `invfreqs` is robust in the sense that it can accurately estimate the spectrum of three or more relaxations, and its convergence is not sensitive to the initial guess. The major downside of this method is that it can return complex spectral amplitudes or negative relaxation frequencies that have no physical meaning.

In this paper, we propose a method of estimating the DSRF that requires no prior knowledge of the model order and always returns real model parameters. The proposed method assumes a nonnegative DSRF. While it has not been proven that the DSRF is nonnegative for all targets, the proposed method works well in practice. Even with the constraint, the proposed method can represent a much larger class of responses than the parametric models such as the Cole–Cole and Havriliak–Negami models. For well-known canonical targets, as presented in this paper, the estimated DSRF is an approximate, if not an exact, representation of the actual physical DSRF.

II. Estimation Method

When the target response is measured at N distinct frequencies, (4) can be written in a matrix form

$$\begin{bmatrix} H(\omega_1) \\ H(\omega_2) \\ \vdots \\ H(\omega_N) \end{bmatrix} = \underbrace{\begin{bmatrix} 1 & \frac{1}{1+j\omega_1/\zeta_1} & \frac{1}{1+j\omega_1/\zeta_2} & \cdots & \frac{1}{1+j\omega_1/\zeta_k} \\ 1 & \frac{1}{1+j\omega_2/\zeta_1} & \frac{1}{1+j\omega_2/\zeta_2} & \cdots & \frac{1}{1+j\omega_2/\zeta_k} \\ \vdots & \vdots & \vdots & \ddots & \vdots \\ 1 & \frac{1}{1+j\omega_N/\zeta_1} & \frac{1}{1+j\omega_N/\zeta_2} & \cdots & \frac{1}{1+j\omega_N/\zeta_k} \end{bmatrix}}_{\boldsymbol{Z}} \begin{bmatrix} c_0 \\ c_1 \\ c_2 \\ \vdots \\ c_k \end{bmatrix}$$

$$\boldsymbol{h} = \boldsymbol{Z}c \tag{5}$$

where $\omega_{\min} = \omega_1 < \omega_2 < \cdots < \omega_N = \omega_{\max}$, $\boldsymbol{h}$ is the observation vector, $\boldsymbol{c}$ is the spectral amplitude vector augmented by the shift c_0, and $\boldsymbol{Z}$ is a matrix containing information about the relaxation frequencies $\boldsymbol{\zeta}$'s. The dimension of the matrix $\boldsymbol{Z}$ is dependent on the number of relaxations present in the spectrum (i.e., the model order). In the case of a simple thin wire circular loop, there is only one relaxation, so $\boldsymbol{Z}$ has two columns; the first column is always one to account for c_0.

A. Method Formulation

To estimate the DSRF (i.e., ζ_k and c_k) from a given observation $\boldsymbol{h}$, the usual approach is to minimize the norm of the error, $\|\boldsymbol{h} - \boldsymbol{Z}\boldsymbol{c}\|$, but this leads to a *nonlinear* optimization problem.

Instead, we follow the strategy of basis pursuit to reformulate (5) as a linear problem with an overcomplete dictionary [26] and then use nonnegative LSQ to select the best basis, i.e., the best $\boldsymbol{\zeta}$. The overcomplete dictionary is actually a matrix $\tilde{\boldsymbol{Z}}$ that has the same form as $\boldsymbol{Z}$ in (5), but with many more columns. To generate the columns, we enumerate a large set of possible relaxation frequencies in log-ζ space and create one column for each enumerated ζ. The enumeration is done by discretizing a range of relaxation frequencies into M sample points $\tilde{\zeta}_m$ that are uniformly distributed in the log-ζ space. The range of relaxation frequencies is chosen such that $\tilde{\zeta}_{\min} \approx \omega_{\min}$ and $\tilde{\zeta}_{\max} \approx \omega_{\max}$. The number M should be chosen large enough to ensure that some $\tilde{\zeta}_m$'s are in close proximity to the actual relaxation frequencies ζ_k's. From our simulations, a good choice of M gives roughly 25 sample points per decade. More discussion on the choice of M can be found in Appendix B.

Since the matrix $\tilde{\boldsymbol{Z}}$ has many more columns than the expected number of relaxations, we define the unknown as an $(M+1)$-element weighted selector vector $\tilde{\boldsymbol{c}}$ and rewrite the problem as

$$\boldsymbol{h} = \tilde{\boldsymbol{Z}}\tilde{\boldsymbol{c}} + error \tag{6}$$

where we expect the solution for $\tilde{\boldsymbol{c}}$ to have many zero elements. The vector $\tilde{\boldsymbol{c}}$ contains the shift estimator $\tilde{c}_0$ followed by the spectral amplitude estimators $\tilde{c}_m$'s. Ideally, when the error between $\boldsymbol{h}$ and $\tilde{\boldsymbol{Z}}\tilde{\boldsymbol{c}}$ is minimized, only those $\tilde{c}_m$'s with corresponding $\tilde{\zeta}_m$'s that are near a true ζ_k will be nonzero, and they will take on the correct spectral amplitudes c_k's. It follows that a DSRF can then be deduced from the nonzero estimated $\tilde{c}_m$'s and their corresponding $\tilde{\zeta}_m$'s.

The challenge in obtaining the correct $\tilde{\boldsymbol{c}}$ is that M is much greater than N, so the system in (6) is underdetermined, and there is not a unique $\tilde{\boldsymbol{c}}$ to minimize the error. Any vector in the null space of $\tilde{\boldsymbol{Z}}$ can be added to $\tilde{\boldsymbol{c}}$ without changing the error. There are many ways to select an LSQ solution. The Moore–Penrose pseudoinverse picks the LSQ solution that has the smallest ℓ_2 norm. One can also compute an LSQ solution with the fewest nonzero components. However, neither of these LSQ solutions produces the correct spectrum. Details about existing techniques and the difficulties of solving such a system can be found in [24], [27], and [28].

In the EMI application, we have found that imposing a nonnegative constraint on $\tilde{\boldsymbol{c}}$ effectively eliminates a large portion of the null space of $\tilde{\boldsymbol{Z}}$ and that the remaining solution space contains reasonable answers. We suggest that the nonnegative constraint can be used where applicable. Mathematically, the DSRF can be found by optimizing

$$\arg\min_{\tilde{\boldsymbol{c}}} \|\tilde{\boldsymbol{Z}}'\tilde{\boldsymbol{c}} - \boldsymbol{h}'\| \qquad \text{subject to } \tilde{\boldsymbol{c}} \geq 0$$

$$\text{where} \quad \tilde{\boldsymbol{Z}}' = \begin{bmatrix} \mathfrak{Re}(\tilde{\boldsymbol{Z}}) \\ \mathfrak{Im}(\tilde{\boldsymbol{Z}}) \end{bmatrix} \quad \text{and} \quad \boldsymbol{h}' = \begin{bmatrix} \mathfrak{Re}(\boldsymbol{h}) \\ \mathfrak{Im}(\boldsymbol{h}) \end{bmatrix}. \tag{7}$$

Separating the real and imaginary parts makes the whole system real. The first element in $\tilde{\boldsymbol{c}}$, i.e., $\tilde{c}_0$, can be guaranteed nonnegative by adding a sufficiently large value to the frequency response $\boldsymbol{h}$.

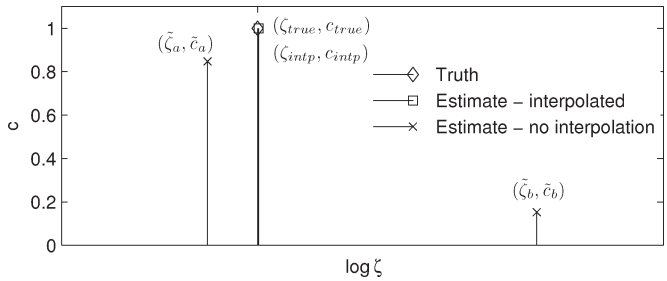

Fig. 1. Splitting of an expected relaxation followed by interpolation. The sample points $\tilde{\zeta}$'s do not coincide with ζ_{true}, so ζ_{true} is split into the two nearest sample points: $\tilde{\zeta}_a$ and $\tilde{\zeta}_b$. The estimation accuracy is increased by interpolating in $\tilde{\zeta}$ using $\tilde{c}_a$ and $\tilde{c}_b$.

B. Implementation

The proposed estimation method can be easily implemented through the function `lsqnonneg` in MATLAB which uses the algorithm found in [29]. An alternative to `lsqnonneg` is the `CVX` package which implements convex optimization under MATLAB [30]. Both optimizers provide satisfactory results. However, `CVX` is a larger and more sophisticated program but is slightly slower than `lsqnonneg` which was written exactly to solve LSQ problems with a nonnegative constraint. Nevertheless, `CVX` would be of great interest if more constraints are to be added.

When using either `lsqnonneg` or `CVX`, we found that normalizing the input data $\boldsymbol{h}$ to have an ℓ_2 norm of unity increases the accuracy of estimation. Therefore, all data will be scaled to an ℓ_2 norm of unity before optimization and scaled back to the original norm after optimization because the original norm may contain useful information for target identification.

C. Interpolation

We observed that, in the estimated DSRF, an expected relaxation $(\zeta_{\text{true}}, c_{\text{true}})$ often gets split into two peaks located at the two sample points adjacent to ζ_{true}, as shown in Fig. 1. We also observed that the two estimated spectral amplitudes add up to the true spectral amplitude c_{true} and that ζ_{true} is closer to $\tilde{\zeta}$ with larger $\tilde{c}$. This phenomenon can be understood: The splitting of relaxation happens when the sample points $\tilde{\zeta}_m$'s do not coincide with ζ_{true}, and c_{true} gets distributed among the two sample points that are the closest to ζ_{true}.

We can increase the accuracy of the estimation by taking advantage of this well-behaved and consistently recurring phenomenon. We can reverse the splitting processes. A true relaxation frequency could be restored by interpolating between two adjacent $\tilde{\zeta}_m$'s with nonzero $\tilde{c}_m$ according to their spectral amplitudes. The interpolated spectral amplitude is simply the sum of the two adjacent spectral amplitudes. Mathematically

$$c_{\text{intp}} = \tilde{c}_a + \tilde{c}_b \tag{8}$$

$$\log(\zeta_{\text{intp}}) = \log(\tilde{\zeta}_a) + \frac{\tilde{c}_b}{\tilde{c}_a + \tilde{c}_b} \log(\tilde{\zeta}_b/\tilde{\zeta}_a). \tag{9}$$

The quantities are shown in Fig. 1. The sample points $\tilde{\zeta}_m$'s are placed close enough that a simple linear interpolation in log-ζ space gives satisfactory results. The interpolation is applied only on two adjacent nonzero relaxations.

After the interpolation is performed, any $\tilde{c}_m$ with a value of zero is eliminated along with its corresponding $\tilde{\zeta}_m$. We denote the resulting relaxation frequencies as $\hat{\zeta}_l$, with spectral amplitudes $\hat{c}_l$, or, in vector notation, as $\hat{\boldsymbol{\zeta}}$ and $\hat{\boldsymbol{c}}$, both with length L. It is convenient and desirable to interpret the estimation results by looking at $\hat{\boldsymbol{\zeta}}$ and $\hat{\boldsymbol{c}}$. Every entry in $\hat{\boldsymbol{\zeta}}$ is an estimate of one relaxation frequency of the target with its corresponding estimated spectral amplitude in $\hat{\boldsymbol{c}}$. The estimated DSRF $\hat{S} = \{(\hat{\zeta}_l, \hat{c}_l) : l = 1, \ldots, L\}$ is then compactly stored in $\hat{\boldsymbol{\zeta}}$ and $\hat{\boldsymbol{c}}$. In addition, the vector length L is an estimate of the model order K. Note that $\tilde{c}_0$ is not part of the DSRF, and therefore not interpolated, and is not in the vector $\hat{\boldsymbol{c}}$.

D. Summary

To estimate the unknown DSRF $S = \{(\zeta_k, c_k)\}$ from a given set of observations $\boldsymbol{h}$ over N frequencies, we first decide on a relaxation frequency range $[\tilde{\zeta}_{\min}, \tilde{\zeta}_{\max}]$ and the number of points M to be sampled in this range. Then, we generate the sample points $\tilde{\zeta}_m$'s, construct a dictionary matrix $\tilde{\boldsymbol{Z}}$, perform the optimization described in (7), and finally obtain the estimated DSRF $\hat{S} = \{(\hat{\zeta}_l, \hat{c}_l)\}$ by interpolating the solution $\tilde{\boldsymbol{c}}$ returned by the optimizer.

In the following three sections, we present the estimation results from synthetic, laboratory, and field data. All estimations are performed with $M = 100$ and optimized with `lsqnonneg`. In assessing the signal strength, the signal-to-noise ratio (SNR) is used. The signal power is computed by $\sum_{i=1}^{N} |H(\omega_i)|^2/N$. The noise power in synthesized data is equal to the variance of the noise. In laboratory and field data, the background signal can be measured and is treated as noise when calculating the SNR. All presented spectra are normalized such that $\sum_{i=1} c_i = 1$ (c_0 is separate). Normalization removes the influence of the signal amplitude which changes for many reasons.

III. Synthetic Data

In this section, the proposed estimation method is tested against synthetic data to show its functionality, robustness, and stability. The synthesized data are sampled at 21 frequencies approximately logarithmically distributed over the range of 300 Hz–90 kHz. The range of ζ for estimation is chosen such that $\log(\tilde{\zeta}_{\min})$ and $\log(\tilde{\zeta}_{\max})$ are 2.4470 and 6.6223, respectively. This corresponds to a frequency range of 45 Hz–670 kHz, which is larger than the measured frequency range. With $M = 100$, the spacing between two sample points is 0.0422 decades. The number of samples and the frequencies are chosen to be the same as an existing hardware system, but the proposed method can also perform under different settings.

1) Notation: ζ and c are the true/theoretical relaxation frequencies and spectral amplitudes; $\hat{\zeta}$ and $\hat{c}$ are the estimates.

A. Dissimilarity Measure Between Two DSRF

Before we can evaluate the goodness of estimation, some kind of measure is needed to assess the dissimilarity between the estimated DSRF and the truth. It is difficult, however, to compare two sparse spectra when the number of relaxations is different, which happens frequently. When the number of relaxations is the same $(K = L)$, a possible measure of the dissimilarity between two spectra is

$$D(\hat{S}, S) = \frac{1}{I}\sum_{i=1}^{I} |\log\hat{\zeta}_i - \log\zeta_i| \qquad \forall\, i \quad \hat{\zeta}_i \le \hat{\zeta}_{i+1} \quad \text{and} \quad \zeta_i \le \zeta_{i+1} \tag{10}$$

where $I = K = L$. In (10), only the relaxation frequencies ζ_k's are considered, and spectral amplitudes c_k's are ignored. This approximation is reasonable and convenient when two spectra are visually similar. We refer to this dissimilarity measure as the deviation. It has the units of decades.

Another measure that is more comprehensive is the Earth Mover's Distance (EMD) [31], [32]. The EMD consistently quantifies the dissimilarity between two spectra, even when $K \neq L$. Intuitively, the EMD measures how much work it takes to morph one spectrum into the other. Specifically, one spectrum represents piles of earth with volume $\hat{c}_l$ located at the associated $\hat{\zeta}_l$. The other spectrum represents holes in the ground with capacity c_k located at ζ_k. The distance between a pile of earth and a hole is naturally defined to be the difference between $\hat{\zeta}_l$ and ζ_k in log space, and the work to move some earth into a hole would be the amount of earth moved times the distance traveled. Then, the EMD is proportional to the least amount of work needed to move as much earth into the holes. For the DSRF, the EMD is measured in decades because it is almost always examined in log-ζ space. See Appendix A for details about the EMD.

B. Two Coplanar Coaxial Loops

We simulate the frequency response for a structure with two coplanar coaxial circular loops of copper wire. A theoretical EMI response and the DSRF of this target are provided in Appendix C. The circumferences of the two loops are chosen to be 200 and 150 mm, respectively. The larger loop has a wire radius of 0.0635 mm (#36 AWG[1]), and the smaller one has a wire radius of 0.3215 mm (#22 AWG). The EMI response is simulated at a 70-dB SNR with additive white Gaussian noise (AWGN). The estimated spectrum is shown in Fig. 2 along with the true spectrum. The estimated spectrum is almost identical to the truth. The deviation from the true spectrum is

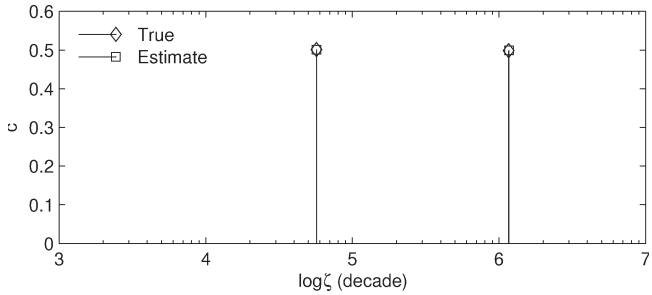

Fig. 2. Estimation of a simulated two coplanar coaxial circular loop target, for which $\log\zeta_k$ and c_k are (4.7552, 6.0651) and (0.5013, 0.4987), respectively. The estimates for log-$\hat{\zeta}_l$ and $\hat{c}_l$ are (4.7557, 6.0672) and (0.5010, 0.4990), respectively.

[1]American wire gauge.

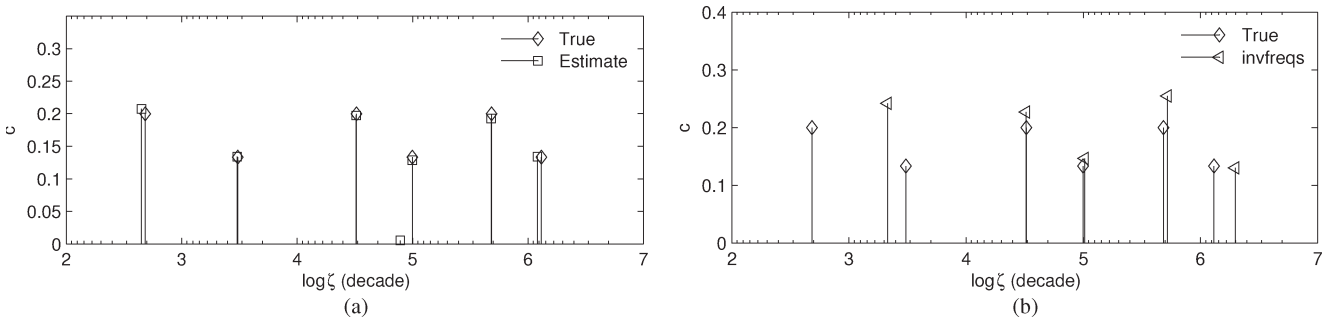

Fig. 3. Estimation of a six-relaxation DSRF. See Table I for numerical data. (a) Estimates by the proposed method. (b) Estimates by `invfreqs` with nonphysical parameters removed.

TABLE I
ESTIMATION OF A SIX-RELAXATION DSRF

Truth	c_k	0.2000	0.1333	0.2000	0.1333	0.2000	0.1333			
	$\log \zeta_k$	2.6842	3.4855	4.5135	4.9985	5.6839	6.1162			
Proposed method	$\hat{c}_l$	0.2076	0.1343	0.1973	0.1286	0.1928	0.1341	0.0052		
	$\log \hat{\zeta}_l$	2.6515	3.4803	4.5109	4.9981	5.6801	6.0809	4.8931		
`invfreqs`	$\hat{c}_l$		0.2418	0.2269	0.1465	0.2546	0.1301	$-0.3902 \cdot 10^{-4}$	$-0.3902 \cdot 10^{-4}$	0.1334
	$\log \hat{\zeta}_l$†		3.3303	4.5111	5.0126	5.7188	6.2983	$-0.0012 + 0.0042i$	$-0.0012 - 0.0042i$	-0.0127

†Negative or complex values are not logged

0.0013 decades, which is very small compared to the detectable ζ range, about 4 decades. The computation took 0.11 s on a 2.66-GHz CPU with 960-MB RAM.

C. Six-Relaxation DSRF

While existing sum-of-exponential estimation methods can also successfully estimate a two-relaxation case, when the number of relaxations is three or more, these methods start to encounter problems such as returning complex model parameters or not converging [24]. We test our method on a six-relaxation DSRF. The target response is synthesized at 70-dB SNR with AWGN

$$H(\omega) = 1 + \sum_{k=1}^{6} \frac{c_k}{1 + j\omega/\zeta_k} + noise. \tag{11}$$

The relaxation frequencies are chosen such that two ζ_k's coincide with a sample point, one ζ_k is half way between two log-ζ sample points, and the rest are randomly in between sample points. The relaxation frequencies are chosen this way to demonstrate the functionality of the proposed method when the sample points do not coincide with the true relaxation frequencies.

The synthesized and estimated DSRFs are shown in Fig. 3(a) and Table I. All six relaxation frequencies are correctly recovered. The estimated model parameters are real, and the deviation from truth is small. The EMD between the estimate and truth is 0.0365 decades. There is a seventh relaxation in the estimate introduced by the noise, but its spectral amplitude is small.

Now, we estimate the DSRF of the same data using `invfreqs`. The *a priori* model order is chosen to be 8 which is slightly higher than the actual but is reasonable because, in practice, it is difficult to know the actual model order. The estimated model parameters are recorded in Table I. There are two estimated ζ's that are complex and one negative. We can try to obtain a physically possible DSRF by throwing away these complex or negative relaxation frequencies. The resulting estimated DSRF is shown in Fig. 3(b). Three relaxations are correctly recovered, but the two left most expected relaxations are not. The EMD between the estimate and truth is 0.3323 decades, much higher than the EMD of the proposed method.

Although a physically possible DSRF can be obtained by throwing away the nonphysical estimates, the resulting spectrum can be quite different from the truth. Using the actual model order or its neighboring numbers as the *a priori* model order does not preclude complex model parameters either. Nevertheless, when the true model order is low and the SNR is high, satisfactory estimates can be obtained from `invfreqs` by throwing out nonphysical parameters.

Returning complex or nonphysical estimates is a problem that plagues many methods, and there is not a proper way to deal with the complex estimates. The best way is perhaps to restrict the model parameters to be real and physical when setting up the problem, and this is the approach taken in the proposed method.

D. SNR

To see how the proposed method performs in noise, a Monte Carlo simulation versus SNR is run on a target with a four-relaxation DSRF. Goodness of estimation is measured by the EMD between the estimate and truth. The simulation result, shown in Fig. 4, shows the robustness of the estimation method at different SNRs.

As expected, the EMD between the estimate and the truth increases as the SNR decreases. This suggests that the proposed method is functional in a range of SNR where the EMD is below some threshold. This threshold, however, depends on the application of the estimated spectrum. For example, in the case of classification, a more robust classifier may tolerate worse estimations and therefore allow lower SNR.

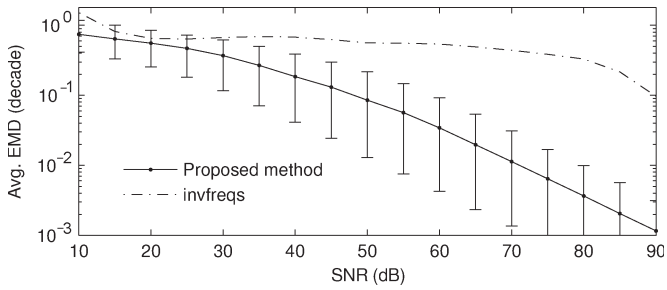

Fig. 4. Monte Carlo simulation on goodness of estimation versus SNR performed on a four-relaxation DSRF. Sample size is 10 000 at each SNR. Error bars indicate the range of EMD between the 10th and 90th percentiles.

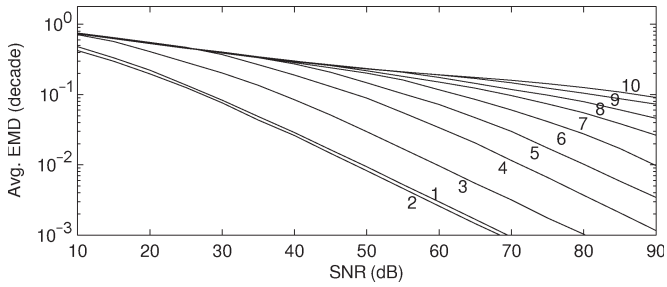

Fig. 5. Monte Carlo simulation on goodness of estimation versus SNR for different DSRFs with model order ranging from 1 to 10. Sample size is 10 000.

The same noise simulation was also performed on `invfreqs` using the actual model order as the *a priori* model order. Nonphysical parameters are removed from the estimate. As shown in Fig. 4, `invfreqs` barely functions except at around 90-dB SNR where its average EMD drops to 0.1 decades. In comparison, the proposed method has an average EMD 100 times smaller than that of `invfreqs` at 90-dB SNR and has low EMD for a wide range of SNR.

In reality, the depth and size of the target are two dominant factors of SNR. The SNR increases with the size of the target and decreases with the buried depth. In our laboratory measurements, a typical SNR for loop targets in this work is 70 dB when the target is placed 10 cm below the EMI sensor.

Fig. 5 shows the same Monte Carlo simulation performed on DSRFs with different model orders using the proposed method. It is seen that a higher model order DSRF requires a higher SNR to achieve a given goodness of fit (EMD). Although the curves are different for each model order, all curves have the same behavior, i.e., the goodness of estimation is positively correlated to the SNR. The consistent trend of these curves suggests that the proposed method is stable and functional over a wide range of SNR.

IV. Laboratory Data

In this section, we are concerned with the physical meaning of the estimated DSRF. We will show that the estimated spectrum agrees with the theoretical and physical DSRFs derived from the electromagnetic theory, and the estimate is not just another good fit to the data, which can be a problem for other estimation methods [24]. The data are measured with a wideband EMI sensor operating at 21 frequencies approximately logarithmically distributed over the range of 300 Hz–90 kHz [33].

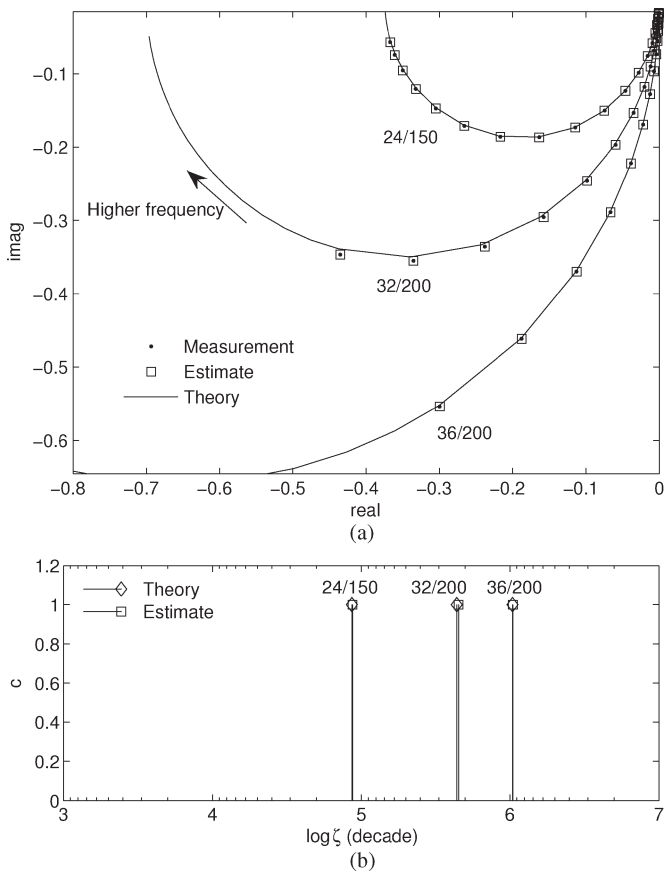

Fig. 6. (a) Frequency response of three independently measured single loops on an Argand diagram. Responses are normalized such that $\|\boldsymbol{h}\|_2 = 1$. Measurements are labeled in the form of AWG/circumference (in millimeters). (b) Theoretical and estimated DSRFs. Theoretical $\log \zeta_k$, from left to right, are 4.9364, 5.6416, and 6.0167. Estimated $\log \hat{\zeta}_l$, from left to right, are 4.9411, 5.6534, and 6.0195. All relaxations have an amplitude of unity.

The frequency response of targets will be presented on Argand diagrams. Specifically, complex frequency response functions are plotted on a complex plane with the imaginary part as the vertical axis, the real part as the horizontal axis, and frequency as the parameter.

A. Single Loop

We first examine the simplest case—a single thin-wire circular loop. The theoretical EMI frequency response and DSRF can be found in [16]. This target contains only one relaxation located at $\zeta = R/L$, where L is the inductance and R is the resistance of the loop. These quantities can be computed according to (19) and (20) in Appendix C.

Fig. 6(a) shows three independently measured EMI responses for circular copper loops of circumferences 150, 200, and 200 mm and AWG Nos. 24, 32, and 36, respectively. The theoretical and estimated DSRFs are shown together in Fig. 6(b). The estimates are seen to agree with the theory. The deviations from the theory are 0.0047, 0.0117, and 0.0028 decades for the loops with AWG Nos. 24, 32, and 36, respectively. All deviations are relatively small in the observable relaxation frequency range, so we conclude that the estimated DSRF is an accurate representation of the physical DSRF.

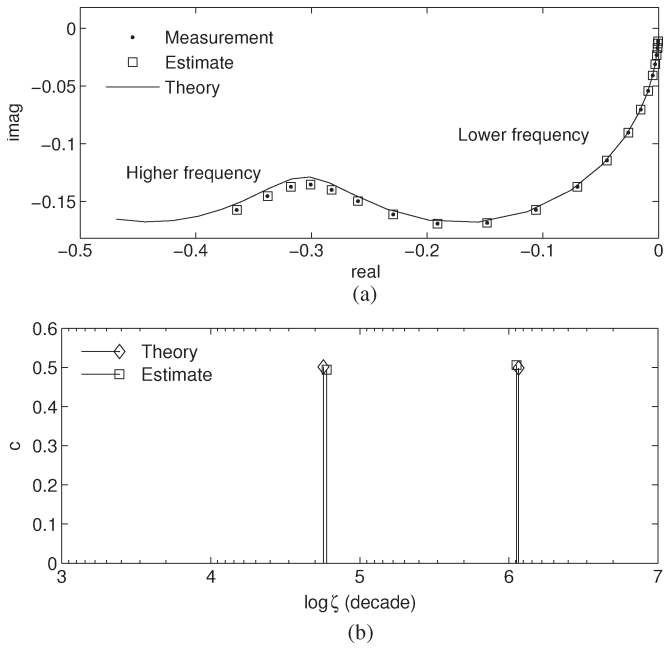

Fig. 7. (a) Laboratory-measured frequency response of two coplanar coaxial circular loops on an Argand diagram. Theory deviates from the measurement at higher frequencies. Responses are normalized such that $\|\boldsymbol{h}\|_2 = 1$. (b) Theoretical and estimated DSRFs. $\log \zeta_k$ and c_k are (4.7552, 6.0651) and (0.5013, 0.4987), respectively. The estimate log-$\hat{\zeta}_l$ and $\hat{c}_l$ are (4.7768, 6.0514) and (0.4941, 0.5059), respectively.

B. Two Coplanar Coaxial Circular Loops

To test the method on a more complicated spectrum, we revisit the case of a target with two coplanar coaxial circular loops considered earlier. A physical target was built according to the same specifications described in Section III-B. The EMI response of this target was measured in the laboratory and is shown in Fig. 7(a). The SNR is about 70 dB. The estimated and theoretical DSRFs are shown in Fig. 7(b).

The estimated DSRF deviates from the theory slightly with a deviation of 0.0177 decades. We believe that this is mostly due to the thin-wire approximation used in the theory. In the theory, the wire radius is assumed to be much smaller than the loop radius. The inner loop (#22 AWG) has a loop radius to wire radius ratio of about of 47 which is not very high, meaning that the wire cannot be modeled as infinitely thin. In addition, thicker wires have a secondary relaxation due to the off-wire-axial current flow which is not accounted for in the theory. At any rate, the deviation is small, and the estimated spectrum is very close to the theory. We can thus conclude that this estimated DSRF is an accurate representation of the true DSRF of the physical target.

C. Nonmagnetic Sphere

The spectrum of a metallic sphere is difficult to estimate because it contains an infinite sequence of relaxations, and the spacing between successive relaxation frequencies decreases as the relaxation frequency decreases [17]. The decrease in spacing makes the relaxations in the region of these closely spaced ζ's indistinguishable from one another. It is therefore understood that it is impossible to perfectly recover the spectrum of a sphere. Here, the proposed method is tested against the EMI response of an aluminum sphere measured in the lab. The sphere has a radius of 0.9525 cm. The theoretical and estimated DSRFs are shown in Fig. 8. The EMD between the truth and estimate is 0.1088 decades.

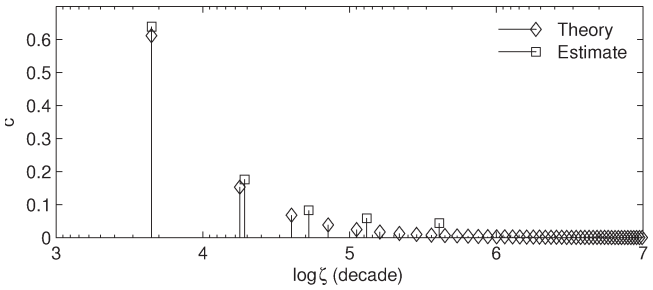

Fig. 8. DSRF estimation of a laboratory-measured sphere. The theoretical DSRF has an infinite sequence of relaxation frequencies.

In the estimated DSRF, the first two relaxations are correctly recovered, but the remaining theoretical relaxations are accounted for by the other three estimated ones. We observed that closely spaced theoretical relaxations in one region are combined into one estimated relaxation, and the theoretical spectral amplitudes in that region roughly add up to the estimated spectral amplitude. For example, the right most estimated relaxation has an amplitude of 0.0438, and it accounts for the infinitely many theoretical relaxations to its right, which have an amplitude sum of 0.0521. The estimated DSRF, even though it cannot recover exactly the theoretical DSRF, is seen to approximate the theory. In this case of a sphere, the estimated DSRF is an approximation to the physical DSRF, and it is not just a good fit, but a fit that can be related to the physical properties of the target.

V. Field Data

As a final demonstration of the proposed method, we estimate the DSRF of three types of landmines (Fig. 9). The EMI measurement system uses a dipole transmit coil and a quadrapole receive coil along with a down-track filter that is important to make the nonnegative constraint applicable for this system [33]. For each type of landmine, measurements were collected from several mines buried at different depths and locations, and the DSRF of each sample was estimated and then plotted together with others of the same type. The spectral amplitudes are represented by the color intensity.

Fig. 9(a) shows the DSRF of seven Type-A mines: low metal content, nonmagnetic, and moderate EMI response antipersonnel mines. The SNR ranges from about 45 to 60 dB. All seven Type-A mines exhibit consistency in the relaxation frequencies and the spectral amplitudes. The average EMD between pairs of mines is 0.0594 decades.

Fig. 9(b) shows the DSRF of eight Type-B mines: medium-metal content, magnetic, and strong EMI response antipersonnel mines. The SNR ranges from about 55 to 70 dB. The spectra are consistent; both $\hat{\boldsymbol{\zeta}}$ and $\hat{\boldsymbol{c}}$ exhibit the same behavior in all eight samples. Mine #7 differs from the others somewhat

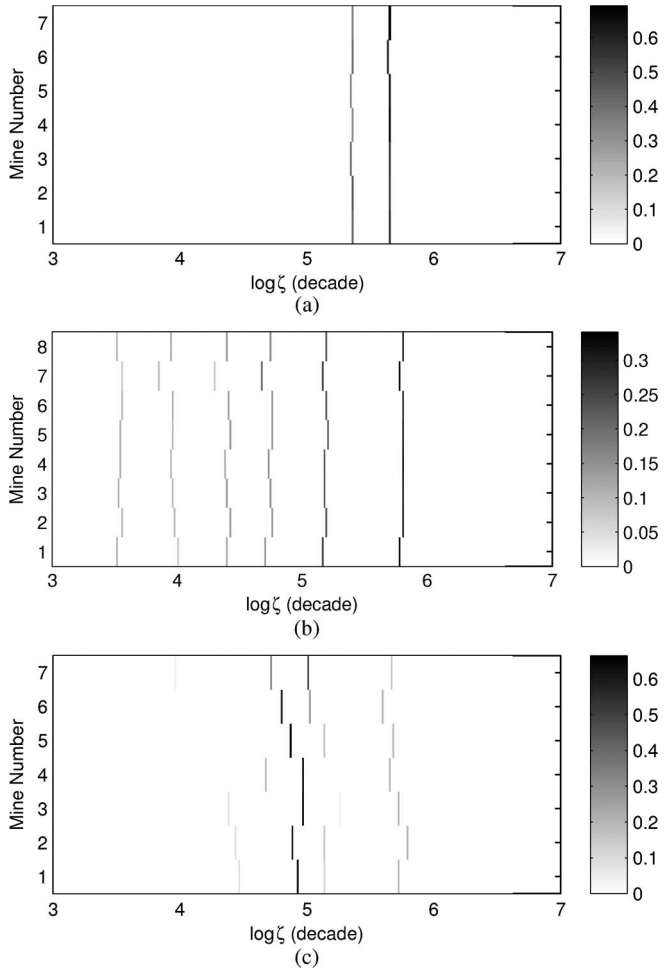

Fig. 9. Estimated DSRF of real landmines. The spectral amplitude is represented by the intensity: The darker the color, larger the amplitude. (a) Seven Type-A mine. (b) Eight Type-B mines. (c) Seven Type-C mines.

in $\hat{\boldsymbol{\zeta}}$, but the number of relaxations and the trend of spectral amplitudes are the same as that of the other seven Type-B mines. The average EMD between pairs of mines is 0.1536 decades.

Fig. 9(c) shows the DSRF of seven Type-C mines: low metal content, magnetic, and weak EMI response antipersonnel mines. The SNR ranges from about 20 to 35 dB. The spectra are less consistent compared to that of Type-A and Type-B mines, but notice that the prominent relaxations are all located around $\log \zeta = 5$ decades. Since the response is weak, the noise could move the relaxations around as observed in Fig. 9(c). The average EMD between mine pairs is 0.1490 decades, which is slightly lower than the average EMD in Fig. 9(b). This is because the two prominent relaxations in Fig. 9(b) are farther away from each other.

The estimated $H(0)$ is normalized and shown in Fig. 10 for the three types of mines. The normalized $H(0)$ reflects the magnetic properties of the mines. Type-A mines are nonmagnetic and therefore have a normalized $H(0)$ close to zero. The other two types of mines have a normalized $H(0)$ well above zero which reflects the magnetic content of the mines. Variations in the estimated $H(0)$ are consistent with the variations in the DSRF.

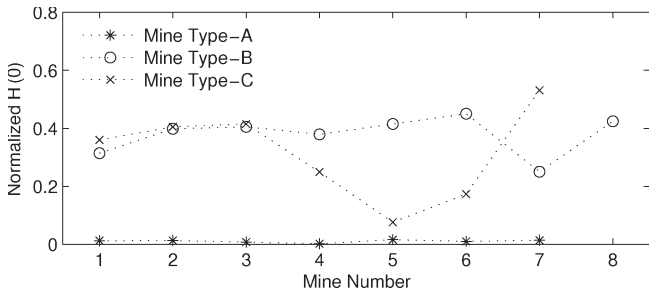

Fig. 10. Normalized estimated $H(0)$ for landmines in Fig. 9. $H(0)$ is normalized by $\sum_{l=1}^{L} \hat{c}_l$.

The variation of the estimated DSRF and $H(0)$ could be caused by several factors such as manufacturing variations, corrosion, the magnetic properties of the soil, or measurement errors. Manufacturing variations in the shape of the metal parts and their electrical and magnetic properties can cause variations in the DSRF. Corrosion can change the properties of the metal parts which will change its response. We believe that mine #7 in Fig. 9(b) has a metal part slightly different from the other seven instances. The lower normalized $H(0)$ suggests a different magnetic property, and the slightly different DSRF reaffirms this small variation in the metal.

The response due to the magnetic properties of the soil can also influence the DSRF since the response of the soil is superimposed on the response of the target and it is not possible to completely separate the two. For the mines shown Fig. 9(c), we believe that the variation in the estimated $H(0)$ is primarily due to the magnetic properties of the soil. Since the magnetic shift observed in the response of the soil is on the same order of magnitude as the response of these mines, the soil can have a strong influence on the mine responses. On the other hand, mines shown in Fig. 9(b) have much stronger EMI responses, and influence from the soil is therefore insignificant.

In general, landmine of one type has consistent estimated DSRFs. These stable and recurring DSRFs could be a valuable feature to be exploited in target discrimination. The estimated $H(0)$ can also be used as a feature when it is not overwhelmed by the noise or ground response.

VI. Conclusion

The proposed method has been tested with a wide variety of data, targets, and noise levels and has been found to give stable, accurate, and quick estimates of the DSRF of a target. When the DSRF cannot be exactly recovered, the estimate is an approximation to the actual. In all cases, the estimated DSRF is directly related to the physical properties of the target, and the same DSRF is robustly estimated in different instances of the same target.

In the future, more work can be put into investigating the applicability of the proposed method, even in other fields of science. In addition, the useful properties that the estimated DSRF possesses suggest that the proposed method would be a promising way to generate features for object identification. More work can be put into designing classifiers based on the estimated DSRF to provide more robust and reliable detectors.

APPENDIX A
EMD

Given two distributions $\hat{S} = \{(\hat{\zeta}_i, \hat{c}_i) : i = 1, \ldots, L\}$ and $S = \{(\zeta_j, c_j) : j = 1, \ldots, K\}$, the EMD between the two distributions can be computed by solving the optimization problem [32]

Define
$$d_{ij} = |\log \hat{\zeta}_i - \log \zeta_j| \tag{12}$$

$$EMD(\hat{S}, S) = \min_{f_{ij}} \frac{\sum_{i=1}^{L}\sum_{j=1}^{K} f_{ij} d_{ij}}{\sum_{i=1}^{L}\sum_{j=1}^{K} f_{ij}} \tag{13}$$

subject to

$$\sum_{j=1}^{K} f_{ij} \le \hat{c}_i, \qquad i = 1, \ldots, L \tag{14}$$

$$\sum_{i=1}^{L} f_{ij} \le c_j, \qquad j = 1, \ldots, K \tag{15}$$

$$\sum_{i=1}^{L}\sum_{j=1}^{K} f_{ij} = \min\left(\sum_{i=1}^{L} \hat{c}_i, \sum_{j=1}^{K} c_j\right) \tag{16}$$

$$f_{ij} \ge 0, \qquad i = 1, \ldots, L;\ j = 1, \ldots, K \tag{17}$$

where f_{ij} is an intermediate variable used during the optimization. Adapting the illustration in Section III-A, $\hat{S}$ is the pile of earth and S denotes the holes. Equation (14) guarantees no overdraw from each pile of earth, (15) guarantees no over fill at each hole, (16) sets the problem to fill up the holes with as much earth as possible, and (17) allows only moving earth into holes and not the reverse.

In our application, spectra should be normalized by having the sum of all spectral amplitudes be unity ($\sum c_i = 1$). In this case, the aforementioned optimization problem is simplified to having the denominator in (13) be one and the right-hand side of (16) be unity. The EMD also becomes symmetric.

APPENDIX B
DENSITY OF DISCRETIZATION OF THE RELAXATION FREQUENCY SPACE

The number M in (5) decides the number of sample points placed in a relaxation frequency range. Equivalently, M controls the density of discretization of the ζ space. The denser the discretization, the more likely the sampled ζ is close to the true ζ. In the extreme case, if an infinite number of sample points fill up the relaxation frequency range, there must be one sampled ζ that coincides with the true ζ. Of course, computationally, it would be impossible to estimate a DSRF with an infinite number of sample points. Even if the number of samples is kept finite, with a fixed number of observations N, the null space of $\tilde{\boldsymbol{Z}}$ gets larger and larger as M increases, and the number of possible bad estimates increases. It is therefore desirable to have M just large enough, so that the estimate is likely correct while the computational cost remains low.

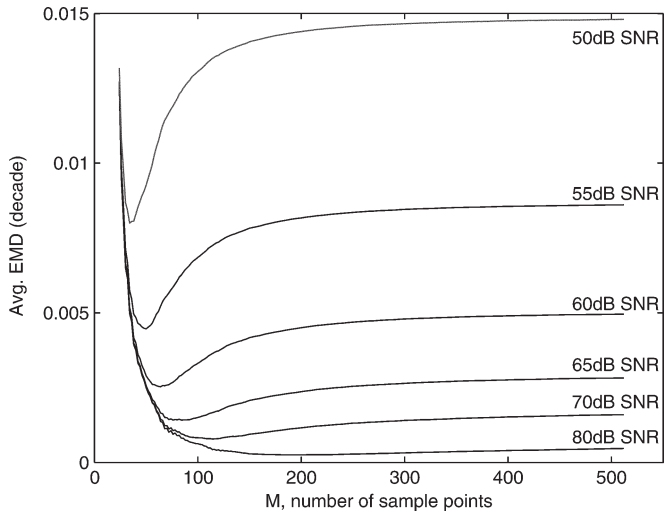

Fig. 11. Monte Carlo simulation on density of discretization of ζ space. Each point on the curve is the average EMD over 10 000 samples.

A Monte Carlo simulation on the density of discretization of ζ space is performed over a range of M with different noise levels. The simulation result is shown in Fig. 11, where a higher EMD value means worse estimates. The figure suggests that M should be greater than 60 to avoid bad estimation due to not enough sample points, while M should be no greater than 200 because adding more sample points does not improve the goodness of fit. We see that within the range $60 < M < 200$, at lower SNRs (50–60 dB), better estimation is obtained with $M \approx 70$. While at higher SNRs (65–80 dB), better estimation is obtained with $M \approx 120$. In other words, at lower SNR, lower discretization density gives more robust performance, which agrees with the intuition that larger dictionaries are more sensitive to perturbation of noise. On the other hand, when the SNR is high, higher discretization density delivers more accurate estimates. To accommodate a wide range of SNR, we compromise to have $M \approx 100$, and since the relaxation frequency range is about 4 decades, there are about 25 sample points per decade.

Although the Monte Carlo simulation is performed on a two-relaxation target, the result should well represent the behavior of the estimation process in general. This is true as observed in simulations of different DSRFs. We can therefore infer that, in general, a good choice of M is around 25 sample points per decade. As shown in the figure, the goodness of fit is not sensitive to the chosen M given it is large enough, so there is some freedom in choosing M.

APPENDIX C
CIRCUIT MODEL FOR TWO COPLANAR COAXIAL CIRCULAR LOOPS

This section derives a theoretical approximation to the magnetic polarizability of two coplanar coaxial circular loops in the low-frequency realm. A larger loop of radius r_1 with wire radius a_1 is placed around a smaller loop of radius r_2 with wire radius a_2. The wires have electric conductivity σ and relative permeability μ_r. Two loops are on the same plane and share the

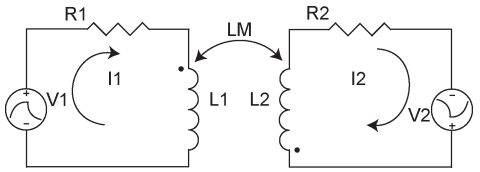

Fig. 12. Circuit model for two coplanar coaxial circular loops.

same center. The wire radius is assumed to be much smaller than the loop radius, i.e., $a \ll r$. This configuration of two coplanar coaxial circular loops can be modeled as a simple two coupled LR circuits shown in Fig. 12.

The voltage $V(s)$ induced by the incident magnetic field on the loop is related to the incident magnetic excitation $H^{\rm inc}$ in Laplace domain through

$$V(s) = -s\mu_0 H^{\rm inc} A \tag{18}$$

where $\boldsymbol{A}$ is the loop area and μ_0 is the permeability of free space. Assume that the incident magnetic field is normal to the plane containing the loops. In low frequency, the resistance R of the loop is

$$R = \frac{2r}{a^2\sigma} \tag{19}$$

and the inductance L is [34]

$$L = r\mu_0 \left[\left(1+\frac{a^2}{8r^2}\right)\ln\left(\frac{8r}{a}\right) + \frac{a^2}{24r^2} - 2 + \frac{\mu_r}{4}\right]. \tag{20}$$

The mutual inductance L_M between the two loops is [35]

$$L_M = \frac{2\mu\sqrt{r_1 r_2}}{k}\left[\left(1-\frac{1}{2}k^2\right)K(k) - E(k)\right] \tag{21}$$

where

$$k^2 = \frac{4r_1 r_2}{(r_1+r_2)^2} \tag{22}$$

and K and E are the complete elliptic integrals.

In Laplace domain, the system equation for the circuit is [16]

$$\begin{bmatrix} V_1 \\ V_2 \end{bmatrix} = \begin{bmatrix} R_1+sL_1 & sL_M \\ sL_M & R_2+sL_2 \end{bmatrix}\begin{bmatrix} I_1 \\ I_2 \end{bmatrix}. \tag{23}$$

Solve for the currents

$$\begin{bmatrix} I_1 \\ I_2 \end{bmatrix} = \frac{-s\mu_0 H^{\rm inc}}{(R_1+sL_1)(R_2+sL_2)-(sL_M)^2} \cdot \begin{bmatrix} R_2+sL_2 & -sL_M \\ -sL_M & R_1+sL_1 \end{bmatrix}\begin{bmatrix} A_1 \\ A_2 \end{bmatrix}. \tag{24}$$

The magnetic polarizability $\mathcal{M}$ is then

$$\mathcal{M}(s) = \frac{A_1 I_1 + A_2 I_2}{H^{\rm inc}} \tag{25}$$

$$= \frac{-s\mu_0\left[A_1^2(R_2+sL_2)+A_2^2(R_1+sL_1)-2sA_1A_2L_M\right]}{(R_1+sL_1)(R_2+sL_2)-(sL_M)^2}. \tag{26}$$

Perform partial fraction expansion

$$\mathcal{M}(s) = -s\left(\frac{Q_1}{s-s_1}+\frac{Q_2}{s-s_2}\right) \tag{27}$$

$$= -(Q_1+Q_2) + \frac{Q_1}{1-s/s_1} + \frac{Q_2}{1-s/s_2} \tag{28}$$

where s_1 and s_2 are the roots of the denominator in (26) [18]

$$s_{1,2} = \frac{-(R_1L_2+R_2L_1) \pm \sqrt{(R_1L_2-R_2L_1)^2+4R_1R_2L_M^2}}{2\,(L_1L_2-L_M^2)}. \tag{29}$$

Variables Q_1 and Q_2 are simply

$$Q_1 = \frac{\mu_0\left[A_1^2(R_2+s_1L_2)+A_2^2(R_1+s_1L_1)-2s_1A_1A_2L_M\right]}{s_1-s_2} \tag{30}$$

$$Q_2 = \frac{\mu_0\left[A_1^2(R_2+s_2L_2)+A_2^2(R_1+s_2L_1)-2s_2A_1A_2L_M\right]}{s_2-s_1}. \tag{31}$$

By using (29)–(31), the DSRF of two coplanar coaxial circular loops can be computed. The relaxation frequency $\zeta_k = -s_k$ with corresponding spectral amplitude Q_k.

ACKNOWLEDGMENT

The authors would like to thank Dr. A. C. Gurbuz for the insightful comments and for suggesting the applicability of CVX and ℓ_1 minimization.

REFERENCES

[1] D. A. Keiswetter, I. J. Won, J. Miller, T. Bell, E. Cespedes, and K. O'Neill, "Discriminating capabilities of multifrequency EMI data," in *Proc. IGARSS*, Honolulu, HI, Jul. 2000, vol. 4, pp. 1415–1417.

[2] P. Gao, L. Collins, P. M. Garber, N. Geng, and L. Carin, "Classification of landmine-like metal targets using wideband electromagnetic induction," *IEEE Trans. Geosci. Remote Sens.*, vol. 38, no. 3, pp. 1352–1361, May 2000.

[3] E. B. Fails, P. A. Torrione, W. R. Scott, Jr., and L. M. Collins, "Performance of a four parameter model for modeling landmine signatures in frequency domain wideband electromagnetic induction detection systems," *Proc. SPIE*, vol. 6553, p. 655 30D, Apr. 2007.

[4] L. Collins, P. Gao, and L. Carin, "An improved Bayesian decision theoretic approach for land minedetection," *IEEE Trans. Geosci. Remote Sens.*, vol. 37, no. 2, pp. 811–819, Mar. 1999.

[5] L. S. Riggs, J. E. Mooney, and D. E. Lawrence, "Identification of metallic mine-like objects using low frequency magnetic fields," *IEEE Trans. Geosci. Remote Sens.*, vol. 39, no. 1, pp. 56–66, Jan. 2001.

[6] J. T. Miller, T. H. Bell, J. Soukup, and D. Keiswetter, "Simple phenomenological models for wideband frequency-domain electromagnetic induction," *IEEE Trans. Geosci. Remote Sens.*, vol. 39, no. 6, pp. 1294–1298, Jun. 2001.

[7] F. S. Grant and G. F. West, *Interpretation Theory in Applied Geophysics*. New York: McGraw-Hill, 1965, ch. 17.

[8] S. H. Ward, "Electromagnetic theory for geophysical applications," in *Mining Geophysics*, vol. 2, D. A. Hansen, W. E. Heinrichs, Jr., R. C. Holmer, R. E. MacDougall, G. R. Rogers, J. S. Sumner, and S. H. Ward, Eds. Tulsa, OK: Soc. Explor. Geophys., 1967, ch. 2, pp. 10–196.

[9] K. S. Cole and R. H. Cole, "Dispersion and absorption in dielectrics. I. alternating current characteristics," *J. Chem. Phys.*, vol. 9, no. 4, pp. 341–351, Apr. 1941.

[10] D. W. Davidson and R. H. Cole, "Dielectric relaxation in glycerol, propylene glycol, and n-propanol," *J. Chem. Phys.*, vol. 19, no. 12, pp. 1484–1490, Dec. 1951.

[11] S. Havriliak and S. Negami, "A complex plane representation of dielectric and mechanical relaxation processes in some polymers," *Polymer*, vol. 8, no. 4, pp. 161–210, 1967.
[12] J. Honerkamp and J. Weese, "A nonlinear regularization method for the calculation of relaxation spectra," *Rheol. Acta*, vol. 32, no. 1, pp. 65–73, Jan. 1993.
[13] E. Barsoukov and J. R. Macdonald, *Impedance Spectroscopy*. Hoboken, NJ: Wiley-Interscience, 2005, ch. 2, p. 37.
[14] A. A. Kaufman and P. A. Eaton, *The Theory of Inductive Prospecting*. Amsterdam, The Netherlands: Elsevier, 2001, ch. 3.
[15] C. E. Baum, "On the singularity expansion method for the solution of electromagnetic interaction problems," Air Force Weapons Lab., Albuquerque, NM, Dec. 1971.
[16] G. D. Sower, "Eddy current responses of canonical metallic targets theory and measurements," EG&G MSI, Albuquerque, NM, May 1997.
[17] C. E. Baum, "Low-frequency near-field magnetic scattering from highly, but not perfectly, conducting bodies," in *Detection and Identification of Visually Obscured Targets*, C. E. Baum, Ed. Philadelphia, PA: Taylor & Francis, 1999, ch. 6, pp. 163–218.
[18] N. Geng, C. E. Baum, and L. Carin, "On the low-frequency natural response of conducting and permeable targets," *IEEE Trans. Geosci. Remote Sens.*, vol. 37, no. 1, pp. 347–359, Jan. 1999.
[19] A. N. Tikhonov, "Solution of incorrectly formulated problems and the regularization method," *Soviet Math. Dokl.*, vol. 4, pp. 1035–1038, Oct. 1963.
[20] R. L. Wolpert, K. Ickstadt, and M. B. Hansen, "A nonparametric Bayesian approach to inverse problems," in *Bayesian Statistics 7*, J. M. Bernardo, A. P. Dawid, J. O. Berger, M. West, D. Heckerman, M. J. Bayarri, and A. F. M. Smith, Eds. Oxford, U.K.: Clarendon, 2003, pp. 403–418.
[21] E. Tuncer and S. M. Gubanski, "On dielectric data analysis. Using the Monte Carlo method to obtain relaxation frequency distribution and comparing non-linear spectral function fits," *IEEE Trans. Dielectr. Elect. Insul.*, vol. 8, no. 3, pp. 310–320, Jun. 2001.
[22] T. K. Sarkar and O. Pereira, "Using the matrix pencil method to estimate the parameters of a sum of complex exponentials," *IEEE Antennas Propag. Mag.*, vol. 37, no. 1, pp. 48–55, Feb. 1995.
[23] M. R. Osborne and G. K. Smyth, "A modified Prony algorithm for exponential function fitting," *SIAM J. Sci. Comput.*, vol. 16, no. 1, pp. 119–138, Jan. 1995.
[24] Y. Das and J. E. McFee, "Limitations in identifying objects from their time-domain electromagnetic induction response," *Proc. SPIE*, vol. 4742, pp. 776–788, Apr. 2002.
[25] E. C. Levy, "Complex-curve fitting," *IRE Trans. Autom. Control*, vol. 4, no. 1, pp. 37–43, May 1959.
[26] S. S. Chen, D. L. Donoho, and M. A. Saunders, "Atomic decomposition by basis pursuit," *SIAM Rev.*, vol. 43, no. 1, pp. 129–159, Aug. 2001.
[27] P. C. Hansen, *Rank-Deficient and Discrete Ill-Posed Problems: Numerical Aspects of Linear Inversion*. Philadelphia, PA: Soc. Ind. Math., 1998.
[28] K. Holmström and J. Petersson, "A review of the parameter estimation problem of fitting positive exponential sums to empirical data," *Appl. Math. Comput.*, vol. 126, no. 1, pp. 31–61, Feb. 2002.
[29] C. L. Lawson and R. J. Hanson, *Solving Least Squares Problems*. Englewood Cliffs, NJ: Prentice-Hall, 1974, ch. 23.
[30] M. Grant, S. Boyd, and Y. Ye, CVX: Matlab Software for Disciplined Convex Programming, Jul. 2008. [Online]. Available: http://www.stanford.edu/~boyd/cvx/
[31] Y. Rubner, C. Tomasi, and L. J. Guibas, "A metric for distributions with applications to image databases," in *Proc. ICCV*, Bombay, India, Jan. 1998, pp. 59–66.
[32] B. Fisher, The Earth Mover's Distance, Oct. 2008. [Online]. Available: http://homepages.inf.ed.ac.uk/rbf/CVonline/LOCAL_COPIES/RUBNER/emd.htm
[33] W. R. Scott, Jr., "Broadband array of electromagnetic induction sensors for detecting buried landmines," in *Proc. IGARSS*, Boston, MA, Jul. 2008, pp. II-375–II-378.
[34] W. R. Smythe, S. Silver, J. R. Whinnery, and D. J. Angelakos, "Electricity and magnetism," in *American Institute of Physics Handbook*, D. E. Gray, Ed. New York: McGraw-Hill, 1963, ch. 5, p. 29.
[35] W. R. Smythe, *Static and Dynamic Electricity*. New York: McGraw-Hill, 1968, ch. 8, p. 335.

Mu-Hsin Wei (S'09), received the B.S. degree in electrical and computer engineering from Georgia Institute of Technology, Atlanta, in 2007. He is currently working toward the Ph.D. degree with the School of Electrical and Computer Engineering, Georgia Institute of Technology.

Waymond R. Scott, Jr. (S'81–M'82–SM'03–F'08) received the B.E.E., M.S.E.E., and Ph.D. degrees from the Georgia Institute of Technology, Atlanta, in 1980, 1982, and 1985, respectively.

In 1986, he joined the School of Electrical and Computer Engineering, Georgia Institute of Technology, as an Assistant Professor, where he is currently a Professor. His research involves the interaction of electromagnetic and acoustic waves with materials. This research spans a broad range of topics, including the measurement of the properties of materials, experimental and numerical modeling, and systems for the detection of buried objects. His research is currently concentrated on investigating techniques for detecting objects buried in the earth. This work has many practical applications, for example, the detection of underground utilities, buried hazardous waste, buried structures, unexploded ordnance, and buried land mines.

James H. McClellan (S'69–M'74–SM'79–F'85) received the B.S. degree in electrical engineering from Louisiana State University, Baton Rouge, in 1969 and the M.S. and Ph.D. degrees from Rice University, Houston, TX, in 1972 and 1973, respectively.

Since 1987, he has been a Professor with the School of Electrical and Computer Engineering, Georgia Institute of Technology, where he is currently the John and Marilu McCarty Chair. He is the coauthor of *Number Theory in Digital Signal Processing*, *Computer Exercises for Signal Processing*, *DSP First: A Multimedia Approach*, and *Signal Processing First*, which received the McGraw-Hill Jacob Millman Award for an outstanding innovative textbook in 2003.

Prof. McClellan was a corecipient of the IEEE Jack S. Kilby Signal Processing Medal in 2004.